

# Ring solitons and soliton sacks in imbalanced fermionic systems

Mats Barkman,<sup>1</sup> Albert Samoilenka,<sup>1</sup> Thomas Winyard,<sup>2</sup> and Egor Babaev<sup>1</sup>

<sup>1</sup>*Department of Physics, Royal Institute of Technology, SE-106 91 Stockholm, Sweden*

<sup>2</sup>*School of Mathematics, University of Leeds, Leeds LS2 9JT, United Kingdom*

We show that in superfluids with fermionic imbalance and uniform ground state, there are solitons representing multiple local minima of the free energy landscape. These solitons have nontrivial soliton-soliton and soliton-vortex interactions and can form complicated bound states in the form of “soliton sacks”.

Solitons have long been understood to have profound consequences for the physical properties of fermionic systems [1–4]. Recently new methods were developed to create and observe solitons in superfluid ultracold atoms [4], opening up a route to explore new regimes and properties [5–9]. We will focus on the existence of solitons in so-called imbalanced fermionic systems. Such superfluids exhibit pairing between fermions with different magnitude of Fermi momenta. For example such pairing has been considered in the context of dense quark matter, [10], mixtures of different ultracold atoms [11–15], and superconductors [16–28]. When the effects of imbalance are strong, the ground state of such a system can spontaneously break translation symmetry, by inducing periodic modulation in the complex order parameter. Two commonly considered inhomogeneous ground states are the Fulde-Ferrell (FF) state [29], which exhibits purely phase modulation, and the Larkin-Ovchinnikov (LO) state [30], which consists of purely density modulation. These two are jointly referred to as FFLO states. Situations where both phase and density modulate, have also been found [13, 28]. Conversely if the imbalance is weak, the ground state remains uniform. In this paper we will show that fermionic imbalance can nonetheless change the properties of the system, even when the ground state is uniform, through the existence of energetically stable solitonic excitations.

The Ginzburg-Landau (GL) free energy has been derived from the microscopic theory for various imbalanced systems [12, 28, 31, 32], where fermionic population imbalance diminishes the coefficient of the second-order gradient term. This leads to the required inclusion of higher order gradient terms. We will use the GL model, originally derived in [31], which has been shown to be sufficient when describing effects far from the boundary [33, 34], where the free energy density reads

$$f = \alpha|\psi|^2 - 2|\psi|^4 + |\psi|^6 - c_1|\nabla\psi|^2 + \frac{c_1}{2}|\nabla^2\psi|^2 + c_2|\psi|^2|\nabla\psi|^2 + \frac{c_2}{8}\left((\psi^*\nabla\psi)^2 + (\psi\nabla\psi^*)^2\right), \quad (1)$$

written in dimensionless units, where the field  $\psi = |\psi|e^{i\varphi}$  is the complex order parameter. The two parameters  $c_1$  and  $c_2$  are positive constants and, for systems with a two-dimensional Fermi-surface are given to be  $c_1 = 8/3$  and  $c_2 = 16/3$  (see supplementary material for details of rescaling). Therefore the model can be described by a single parameter  $\alpha$ , which depends on both the temperature and the population imbalance of the system.

Since the second order gradient term is strictly negative, there exists the possibility of non-uniform ground states. This can be seen in the two-dimensional model, where the configuration that minimises the free energy transitions from a uniform state  $\psi = \psi_U$ , where  $|\psi_U|^2 = (2 + \sqrt{4 - 3\alpha})/3$ , to a density-modulating LO state at  $\alpha_c^{\text{LO}} \simeq 0.857$ . This inhomogeneous state minimizes the free energy until the transition to the normal state at  $\alpha = 4/3$ . We note that the soliton solutions we find, exist for the parameter region  $0.56 \lesssim \alpha < \alpha_c^{\text{LO}}$ , which is comparable to the size of the LO regime.

One feature to note regarding Eq. (1), is that it is mathematically related to the Swift-Hohenberg equation, which is also described by a fourth order partial differential equation. This model, initially formulated in the context of thermal convection [35], is commonly used to model pattern formation. The main differences between the GL model described by Eq. (1) and the standard Swift-Hohenberg equation are that the order parameter  $\psi$  is complex-valued and there is an additional coupling between the field strength and the gradient in the terms proportional to  $c_2$  in Eq. (1). A more detailed comparison between the models can be found in the supplementary material.

We turn now to the numerical solutions of the free energy in Eq. (1). We used the nonlinear conjugate gradient flow method both in finite element (FreeFEM [36]) and finite difference schemes, which produced consistent results.

We find numerically that the two-dimensional GL free energy defined by the density in Eq. (1) has a number of local minima, in the form of solitons. The simplest subset of these soliton solutions retain the rotational spatial symmetry of the model, which we coin “ring solitons”. These radial solutions take the form  $\psi = g(r)e^{i\varphi}$  where  $\varphi$  is a constant and  $g(r)$  is a real profile function that modulates continuously between being positive and negative, before decaying to its ground state value  $\pm|\psi_U|$  as  $r \rightarrow \infty$ . This leads us to characterise the solutions by the number of radial nodes ( $g(r) = 0$ ) they exhibit ( $N$ ). In the cases where  $\varphi$  is constant, we assume without loss of generality that  $\varphi = 0$  and thus  $\psi$  is a real field. The  $N = 1$  solutions are displayed in FIG. 1 where  $\psi(r)$  changes sign once. It is important to note that the energy density deviation from the uniform state, plotted for  $\alpha = 0.7$  in FIG. 1, decays such that the total soliton energy is finite. This means that, since entropy scales with system size, solitons will be thermally induced in the thermodynamic limit.

We found stable solutions for  $\alpha \geq \alpha_{c1} \simeq 0.56$ , which suggests that a system with sufficiently weak imbalance will not support these solitonic excitations. As  $\alpha$  increases, the size of

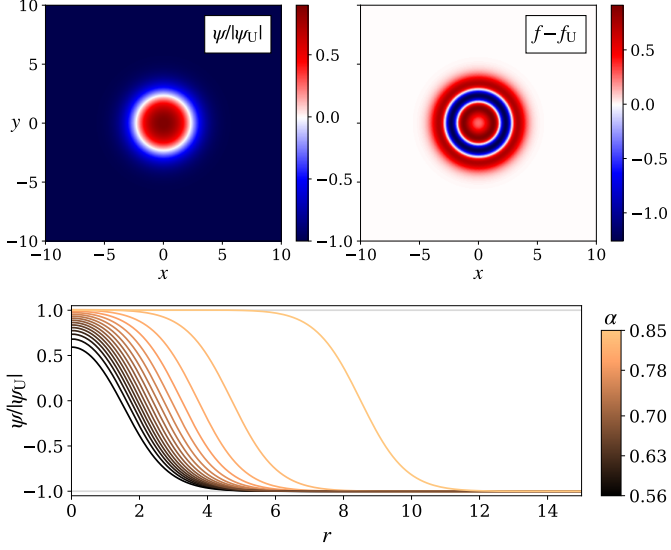


FIG. 1: The two upper panels show (left) the order parameter and (right) the deviation of the free energy density from the uniform ground state, for a ring soliton with one nodal ring ( $N = 1$ ) for  $\alpha = 0.7$ . The lower panel shows cross-sections of the order parameter, for multiple values of  $\alpha$ , of  $N = 1$  solutions, which were found to be stable for  $\alpha \geq \alpha_{c1} \simeq 0.56$ . The nodal radius increases with  $\alpha$ , such that for significantly large  $\alpha$ , the order parameter interpolates between the two ground state values  $\pm|\psi_U|$ .

the soliton also increases, and the order parameter approaches  $|\psi_U|$  at the center of the soliton.

For higher values of  $\alpha$  we find that  $N > 1$  solutions become stable, first at  $\alpha = \alpha_{c2} \simeq 0.733$  for  $N = 2$ , followed by solutions with three and four nodal rings ( $N = 3, 4$ ) at  $\alpha_{c3} \simeq 0.784$  and  $\alpha_{c4} \simeq 0.806$  respectively. The  $N = 1$  to 4 solutions are plotted in figure FIG. 2 along with their energies and increasing nodal radii  $R$  (i.e.  $\psi(R) = 0$ ). The  $N = 1$  solution has the lowest excitation energy above the constant ground state. As the LO transition is approached ( $\alpha \rightarrow \alpha_c^{\text{LO}}$ ) the energies decrease, becoming zero relative to the constant ground state at the transition. At  $\alpha = \alpha_c^{\text{LO}}$ , a state that modulates between the vacua values indefinitely become stable, similar to the LO modulating ground state. Therefore, despite only presenting solutions with four or less nodal rings, we expect that as the FFLO transition is approached, solutions with any number of concentric nodal rings become stable. Namely, for all natural numbers  $N$ , there exists an  $\alpha_{cN}$  such that for  $\alpha \in (\alpha_{cN}, \alpha_c^{\text{LO}})$ , a solitonic excitation with  $N$  concentric nodal rings is stable.

Surprisingly the radial configurations of solitons that we found numerically can be approximated by a simple logistic function to reasonable accuracy. We first note that the LO state can be approximated as successive kink-like modulations. We can then approximate the transition value  $\alpha_c^{\text{LO}}$  to the LO state, by calculating when it is energetically favourable for a single kink-like modulation to appear. Namely when the total en-

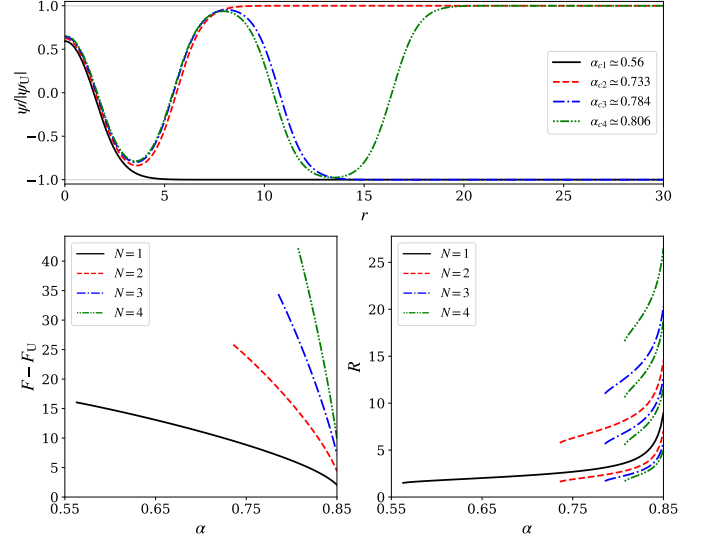


FIG. 2: The upper panel shows radial solutions with  $N$  concentric nodal circles, evaluated at the corresponding value of  $\alpha$  they become stable  $\alpha_{cN}$ . The associated excitation energy  $F - F_U$  (left) and nodal radii  $R$  (right) of these solutions, as a function of  $\alpha$ , is shown in the lower panels. As  $\alpha$  increases (the LO transition is approached), the excitation energy of the soliton approaches zero and its nodal radii diverges.

ergy deviation from the constant ground state, of an infinite system, minimised with respect to  $q$ , of  $\psi = \psi_U \tanh(qx)$  becomes zero. This was calculated to be  $\alpha \simeq 0.858$ , which is remarkably close to the numerically computed value  $\alpha_c^{\text{LO}} \simeq 0.857$ . This in turn leads us to approximate the  $N = 1$  soliton in a similar way, by a radial kink-like profile  $\psi = \psi_U (\tanh q(r + R) - \tanh q(r - R) - 1)$ . If we then substitute this approximation into Eq. (1), the total energy and nodal radius, when numerically minimised with respect to  $q$  and  $R$ , is within an average of 1% of the true numerical solution. Nonetheless, this approximation does not capture the asymptotics of the solution well.

We can understand the stability and nature of these solitons by considering a crude approximation. Consider an  $N = 1$  soliton in the vicinity of the LO phase transition ( $\alpha \lesssim \alpha_c^{\text{LO}}$ ). Inspecting the numerical solutions in FIG. 1 suggests the approximation that  $\psi \simeq \pm|\psi_U|$  everywhere except for a small finite region centred on the nodal radius  $R$ . We then approximate the various terms of the energy density as being independent of  $R$ , except for  $\nabla^2\psi \simeq \partial_r^2\psi + \frac{\partial_r\psi}{R}$ . We reiterate that this crude approximation is valid only when the nodal radius  $R$  is large due to being close to the LO transition. This gives the total excitation energy  $F - F_U \propto \int \left( AR + B + \frac{C}{R} \right) dr$ , where  $A$ ,  $B$  and  $C$  depend on  $\psi$ . These terms then have the following physical interpretation:  $A_{\text{tot}} = \int A dr$  corresponds to the energy per unit length of a straight nodal line, which in a uniform ground state is positive. Hence its contribution to the energy decreases as the radius  $R$  becomes smaller. This shrinking

is balanced by the term  $C_{\text{tot}} = \int C dr$  (where  $C \propto (\partial_r \psi)^2$ ) which represents the energy cost associated with increasing the curvature of the nodal ring  $\propto \frac{1}{R}$ . These competing contributions lead to stable ring solitons with  $R \simeq \sqrt{\frac{C_{\text{tot}}}{A_{\text{tot}}}}$ . Note, that  $R \rightarrow \infty$  as  $\alpha \rightarrow \alpha_c^{\text{LO}}$ , due to  $A_{\text{tot}} \rightarrow 0$  in this limit. The argument above can be extended to  $N > 1$ , demonstrating that solitons with any number of nodal rings are expected to be stable if  $\alpha$  is sufficiently close to  $\alpha_c^{\text{LO}}$ .

We can understand the long range nature of the solutions by considering the linearised theory. We consider the field far from the soliton centre, such that we can write it as a small perturbation about its ground state  $\psi = \psi_U + \varepsilon$ . By assuming that any terms of order  $O(\varepsilon^2)$  or higher are negligible, we acquire the tractable linearised equation, described in detail in the supplementary material. The solution to this linearised equation gives the asymptotic form of the field as,

$$\varepsilon = \text{Re} \left[ C H_0^{(1)}(\mu r) \right], \quad (2)$$

where  $H_0^{(1)}$  is the zeroth order Hankel function of the first kind and  $C$  is a complex constant. In our model  $\mu = \mu_R + i\mu_I = \sqrt{a + i\sqrt{b - a^2}}$  with  $a = 1 - \frac{5c_2}{4c_1}|\psi_U|^2$  and  $b = 2(\alpha - 12|\psi_U|^2 + 15|\psi_U|^4)$ . For our parameters we have that  $\mu_R$  and  $\mu_I$  are positive. Note, that  $\varepsilon \rightarrow C_\infty \frac{e^{-\mu_I r}}{\sqrt{r}} \cos(\mu_R r + \phi_\infty)$  for  $r \rightarrow \infty$ , where  $C_\infty$  and  $\phi_\infty$  are some real constants. Hence the tails of the solitons decay exponentially over the length scale  $1/\mu_I$ , while their amplitude oscillates with period  $2\pi/\mu_R$ . This effect is present in the states shown in FIG. 1, but becomes visible only if the axes scales are changed. One can interpret this oscillatory decay as a complex coherence length, as discussed in the context of other superconducting models [37].

As we understand the asymptotic form of the solitons we can approximate the long-range inter-soliton forces. We do this by considering two point sources that replicate the asymptotic fields of the interacting solitons and calculate the interaction energy between them [38]. The total deviation from the ground state is given by the superposition of the two asymptotic fields (given in Eq. (2)) with constants  $C^{(1)}$  and  $C^{(2)}$ , located at  $\mathbf{x}_1$  and  $\mathbf{x}_2$  respectively, where the distance  $|\mathbf{x}_1 - \mathbf{x}_2|$  is large. Details of the calculations are given in the supplementary material. This gives the interaction energy

$$F_{\text{int}} = -4c_1 \sqrt{b - a^2} \text{Re} \left[ C^{(1)} C^{(2)} H_0^{(1)}(\mu |\mathbf{x}_1 - \mathbf{x}_2|) \right], \quad (3)$$

which is an oscillating function of separation distance. This predicts that there will be weakly bound states with period  $2\pi/\mu_R$  for solitons at large distances.

It is interesting to compare the radial solitons reported here with the related, yet distinct, radial solutions to the stationary Swift-Hohenberg (SH) equation [39, 40]. The similarity is that both solutions exhibit stable radial oscillations. Apart

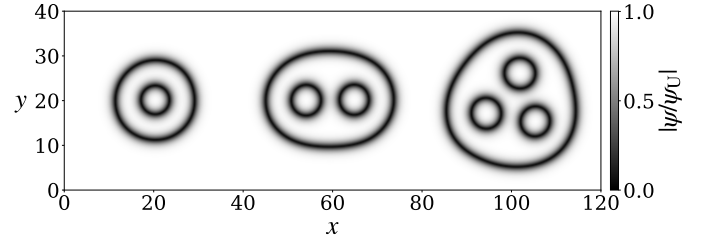


FIG. 3: The state to the left is the  $N = 2$  soliton, where the simplest soliton ( $N = 1$ ) is surrounded by an additional nodal ring. The middle and right states are composite objects, where multiple  $N = 1$  solitons are confined by an outer nodal ring. We call these composite structures soliton sacks. All solutions above were computed at  $\alpha = 0.825$ .

from the previously mentioned differences (complex order parameter and the additional terms proportional to  $c_2$  in Eq. (1)), there is a key difference in that the ground state in [39, 40] is the homogeneous solution  $\psi = 0$ , around which the solutions oscillate. In contrast the nonlinear part of our solution modulate between two antipodal points on the  $U(1)$  ground state manifold. At large distances, both the SH and our solutions decay exponentially, exhibiting oscillatory tails.

We find however that radially symmetric solutions, represent only a small fraction of the solitonic solutions in the model described by Eq. (1). Namely, as the LO transition is approached, we find more structurally complicated solutions that break rotational symmetry, examples of which are plotted in FIG. 3. These can be interpreted as soliton sacks, where a larger soliton confines a group of smaller solitons. This confinement is a completely nonlinear effect and cannot be explained by the asymptotic inter-soliton forces. Such solutions are reminiscent of the ostensibly unrelated Skymion sack/bag solutions, which attract substantial interest in chiral superconductors [41, 42] and magnets [43, 44].

While we have demonstrated a rich spectrum of new solutions in imbalanced systems, the natural question is how they interact with the familiar soliton excitations, namely vortices. We consider a regime away from the LO instability (exemplified by the choice  $\alpha = 0.7$ ) where ordinary vortex solutions exist (namely away from the regime where a vortex core induced FFLO state reported in [45]). We find that the solitons and vortices form bound states, shown in FIG. 4. The energy of this bound state is lower than the combined energy of a separate single vortex and soliton, but the energy of the bound state is larger than the energy of a single ordinary vortex.

Finally our results prompt the question of whether or not these solitons exist over the background of another imbalanced state with uniform density: namely the Fulde-Ferrell (FF) state, where the background phase modulates. An example of a microscopically derived Ginzburg-Landau model for the FF state can be found in [32]. To model the FF state, without fine-tuning, we chose parameters  $\alpha = 0.5$ ,  $c_1 = 2$  and  $c_2 = 2$  phenomenologically. Our numerical studies suggested

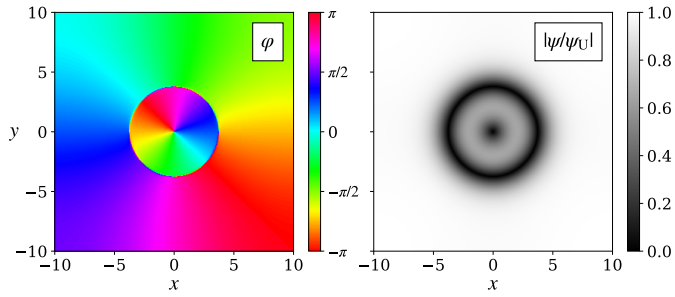


FIG. 4: A bound state of a vortex and a soliton, at  $\alpha = 0.7$ . At the nodal line of the soliton the vorticity receives a  $\pi$  phase shift. The energy of this composite topological defect is smaller than the energy of infinitely separated vortex and soliton.

that the solitons described above, are not stable on top of the FF ground state  $\psi_{\text{FF}} = |\psi_{\text{FF}}|e^{iqy}$ . However that the Fulde-Ferrell state has its own stable solitonic excitations of a different kind: vortex-antivortex pairs. In contrast we did not observe such a solution outside of the FF regime. In FIG. 5 we show a stable vortex-antivortex pair and examples of the possible structures that can be formed by multiple pairs.

In conclusion, we have shown that fermionic imbalance leads to solitonic excitations. These solitons constitute a number of local minima of the free energy landscape and should be observable in a fluctuating, quenched or driven system. Some of the solutions we find are related, but distinctly different, to solutions of the Swift-Hohenberg equation. The solitons have nontrivial interactions, leading to multi-solitonic bound states, soliton sacks and composite vortex-soliton excitations. In ultracold atoms, such states could be created and observed by imprinting methods and standard density-sensitive techniques. In a superconductor, such solitons could be observed via scanning tunneling microscopy in superconducting films subjected to in-plane magnetic fields.

#### ACKNOWLEDGEMENTS

We thank Andrea Benfenati and Martin Speight for useful discussions. The work was supported by the Swedish Research Council Grants No. 642-2013-7837, 2016-06122, 2018-03659, the Göran Gustafsson Foundation for Research in Natural Sciences and Medicine, Olle Engkvists Stiftelse, and the UK Engineering and Physical Sciences Research Council through grant EP/P024688/1. The computations were performed on resources provided by the Swedish National Infrastructure for Computing (SNIC) at the National Supercomputer Center in Linköping, Sweden.

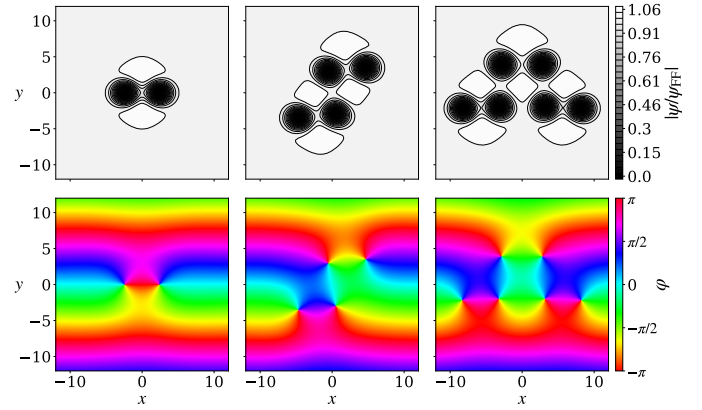


FIG. 5: Solitonic excitations in Fulde-Ferrell (FF) state: stable vortex-antivortex pairs. The pairs have long-range attractive interaction like in an ordinary superfluid, but in the FF background are protected from decay by a potential barrier. The solutions are shown for the GL model in Eq. (1) with  $\alpha = 0.5$  and  $c_1 = c_2 = 2$ .

- [2] A. J. Heeger, S. Kivelson, J. R. Schrieffer, and W. P. Su, *Rev. Mod. Phys.* **60**, 781 (1988).
- [3] J. Goldstone and F. Wilczek, *Physical Review Letters* **47**, 986 (1981).
- [4] T. Yefsah, A. T. Sommer, M. J. Ku, L. W. Cheuk, W. Ji, W. S. Bakr, and M. W. Zwierlein, *Nature* **499**, 426 (2013).
- [5] R. M. Lutchyn, M. Dzero, and V. M. Yakovenko, *Physical Review A* **84**, 033609 (2011).
- [6] D. K. Efimkin and V. Galitski, *Physical Review A* **91**, 023616 (2015).
- [7] M. J. Ku, B. Mukherjee, T. Yefsah, and M. W. Zwierlein, *Physical review letters* **116**, 045304 (2016).
- [8] T. Ren and I. Aleiner, *Physical Review A* **99**, 013626 (2019).
- [9] S. Dutta and E. J. Mueller, *Physical review letters* **118**, 260402 (2017).
- [10] M. Alford, J. A. Bowers, and K. Rajagopal, *Physical Review D* **63**, 074016 (2001).
- [11] M. W. Zwierlein, *Science* **311**, 492 (2006).
- [12] L. Radzihovsky, *Phys. Rev. A* **84**, 023611 (2011).
- [13] A. Samoilienka, F. N. Rybakov, and E. Babaev, *Physical Review A* **101**, 013614 (2020).
- [14] A. Bulgac and M. M. Forbes, *Physical review letters* **101**, 215301 (2008).
- [15] L. Radzihovsky and D. E. Sheehy, *Reports on Progress in Physics* **73**, 076501 (2010).
- [16] A. Bianchi, R. Movshovich, C. Capan, P. G. Pagliuso, and J. L. Sarrao, *Phys. Rev. Lett.* **91**, 187004 (2003).
- [17] C.-w. Cho, J. H. Yang, N. F. Q. Yuan, J. Shen, T. Wolf, and R. Lortz, *Phys. Rev. Lett.* **119**, 217002 (2017).
- [18] S. Uji, Y. Iida, S. Sugiura, T. Isono, K. Sugii, N. Kikugawa, T. Terashima, S. Yasuzuka, H. Akutsu, Y. Nakazawa, D. Graf, and P. Day, *Physical Review B* **97**, 1 (2018).
- [19] H. Mayaffre, S. Krämer, M. Horvatić, C. Berthier, K. Miyagawa, K. Kanoda, and V. F. Mitrović, *Nature Physics* **10**, 928 (2014), arXiv:arXiv:1409.0786v1.
- [20] W. A. Coniglio, L. E. Winter, K. Cho, C. Agosta, B. Fravel, and L. Montgomery, *Physical Review B* **83**, 224507 (2011).
- [21] M. Norman, *Physical review letters* **71**, 3391 (1993).

[1] R. Jackiw and C. Rebbi, *Physical Review D* **13**, 3398 (1976).

- [22] K. Cho, H. Kim, M. Tanatar, Y. Song, Y. Kwon, W. Coniglio, C. Agosta, A. Gurevich, and R. Prozorov, *Physical Review B* **83**, 060502 (2011).
- [23] Y. Matsuda and H. Shimahara, *Journal of the Physical Society of Japan* **76**, 051005 (2007).
- [24] R. Lortz, Y. Wang, A. Demuer, P. Böttger, B. Bergk, G. Zwicknagl, Y. Nakazawa, and J. Wosnitza, *Physical review letters* **99**, 187002 (2007).
- [25] J. Singleton, J. Symington, M. Nam, A. Ardavan, M. Kurmoo, and P. Day, *Journal of Physics: Condensed Matter* **12**, L641 (2000).
- [26] C. Martin, C. Agosta, S. Tozer, H. Radovan, E. Palm, T. Murphy, and J. Sarrao, *Physical Review B* **71**, 020503 (2005).
- [27] D. F. Agterberg, E. Babaev, and J. Garaud, *Physical Review B - Condensed Matter and Materials Physics* **90**, 1 (2014), arXiv:1403.6655.
- [28] M. Barkman, A. A. Zyuzin, and E. Babaev, *Physical Review B* **99**, 220508 (2019).
- [29] P. Fulde and R. A. Ferrell, *Physical Review* **135**, 550 (1964).
- [30] A. I. Larkin and Y. N. Ovchinnikov, *Zh. Eksp. Teor. Fiz.* **47**, 1136 (1964), [*Sov. Phys. JETP*20,762(1965)].
- [31] A. I. Buzdin and H. Kachkachi, *Physics Letters A* **225**, 341 (1997).
- [32] D. Agterberg and K. Yang, *J. Phys.: Condens. Matter* **13**, 9259 (2001).
- [33] M. Barkman, A. Samoilenska, and E. Babaev, *Phys. Rev. Lett.* **122**, 165302 (2019).
- [34] A. Samoilenska, M. Barkman, A. Benfenati, and E. Babaev, *Phys. Rev. B* **101**, 054506 (2020).
- [35] J. Swift and P. C. Hohenberg, *Physical Review A* **15**, 319 (1977).
- [36] F. Hecht, *J. Numer. Math.* **20**, 251 (2012).
- [37] M. Speight, T. Winyard, and E. Babaev, *Physical Review B* **100**, 174514 (2019).
- [38] J. M. Speight, *Phys. Rev. D* **55**, 3830 (1997).
- [39] H. Sakaguchi and H. R. Brand, *Physica D: Nonlinear Phenomena* **97**, 274 (1996).
- [40] D. Lloyd and B. Sandstede, *Nonlinearity* **22**, 485 (2009).
- [41] J. Garaud, J. Carlström, and E. Babaev, *Physical review letters* **107**, 197001 (2011).
- [42] J. Garaud, J. Carlström, E. Babaev, and M. Speight, *Physical Review B* **87**, 014507 (2013).
- [43] D. Foster, C. Kind, P. J. Ackerman, J.-S. B. Tai, M. R. Dennis, and I. I. Smalyukh, *Nature Physics* **15**, 655 (2019).
- [44] F. N. Rybakov and N. S. Kiselev, *Phys. Rev. B* **99**, 064437 (2019).
- [45] D. Inotani, S. Yasui, T. Mizushima, and M. Nitta, “Radial fulde-ferrell-larkin-ovchinnikov state in a population-imbalanced fermi gas,” (2020), arXiv:2003.03159 [cond-mat.quant-gas].

## Supplementary Material: Ring solitons and soliton sacks in imbalanced fermionic systems

### RESCALING OF MICROSCOPICALLY DERIVED GINZBURG-LANDAU ENERGY FUNCTIONAL

In this study we use the Ginzburg-Landau free energy expansion derived in [31], starting from a microscopic model for a spin-imbalanced superfluid. The resulting free energy functional reads

$$F = \int d^d x \left\{ \alpha |\Delta|^2 + \beta |\nabla \Delta|^2 + \gamma |\Delta|^4 + \delta |\nabla^2 \Delta|^2 + \mu |\Delta|^2 |\nabla \Delta|^2 + \frac{\mu}{8} \left( (\Delta^* \nabla \Delta)^2 + (\Delta \nabla \Delta^*)^2 \right) + \nu |\Delta|^6 \right\} \quad (\text{S.1})$$

where  $\Delta$  is the superfluid order parameter and the coefficients  $\alpha, \beta, \gamma, \mu, \nu$  are functions of the temperature  $T$  and the Zeeman splitting  $H$ . The coefficients  $\alpha, \gamma$ , and  $\nu$  are given by

$$\alpha = -\pi N(0) \left( \frac{1}{\pi} \ln \frac{T_c}{T} + K_1(H, T) - K_1(0, T_c) \right), \quad \gamma = \frac{\pi N(0) K_3(H, T)}{4}, \quad \nu = -\frac{\pi N(0) K_5(H, T)}{8}, \quad (\text{S.2})$$

where  $N(0)$  is the electron density of states at the Fermi surface,  $T_c$  is the critical temperature at  $H = 0$  and

$$K_n(H, T) = \frac{2T}{(2\pi T)^n} \frac{(-1)^n}{(n-1)!} \text{Re} [\Psi^{(n-1)}(z)], \quad (\text{S.3})$$

where  $z = \frac{1}{2} - i \frac{H}{2\pi T}$  and  $\Psi^{(n)}$  is the polygamma function of order  $n$ . The remaining coefficients are given in terms of  $\gamma$  and  $\nu$  as  $\beta = \hat{\beta} v_F^2 \gamma$ ,  $\delta = \hat{\delta} v_F^4 \nu$ , and  $\mu = \hat{\mu} v_F^2 \nu$ , where  $v_F$  is the Fermi velocity and  $\hat{\beta}, \hat{\delta}, \hat{\mu}$  are positive constants that depend on the dimensionality  $d$  of the Fermi surface. The numerical values of  $\hat{\beta}, \hat{\delta}, \hat{\mu}$  in one, two and three dimensions are given in TABLE S1. The possibility of inhomogeneous ground states arise in the parameter regime in which the gradient coefficient  $\beta$  is negative. Since  $\beta$  shares sign with the quartic coefficient  $\gamma$ , the inclusion of positive higher order terms, both in density and momentum, is necessary.

For convenience we perform the following rescaling

$$\psi = \frac{\Delta}{|\Delta_0|}, \quad \tilde{\alpha} = \frac{\alpha}{\alpha_0}, \quad \tilde{x} = q_0 x, \quad F = \frac{\alpha_0 |\Delta_0|^2}{q_0^d} \tilde{F}, \quad (\text{S.4})$$

where  $|\Delta_0|^2 = \frac{-\gamma}{2\nu}$ ,  $\alpha_0 = \frac{\gamma^2}{4\nu}$ ,  $q_0^2 = \frac{-\beta}{2\delta}$  and the rescaled free energy  $\tilde{F}$  reads

$$\tilde{F} = \int d^d \tilde{x} \left\{ \tilde{\alpha} |\psi|^2 - 2|\psi|^4 + |\psi|^6 - c_1 |\tilde{\nabla} \psi|^2 + \frac{c_1}{2} |\tilde{\nabla}^2 \psi|^2 + c_2 |\psi|^2 |\tilde{\nabla} \psi|^2 + \frac{c_2}{8} \left( (\psi^* \tilde{\nabla} \psi)^2 + (\psi \tilde{\nabla} \psi^*)^2 \right) \right\}, \quad (\text{S.5})$$

where  $\tilde{\nabla}$  denotes the gradient with respect to  $\tilde{x}$  and  $c_1 = \frac{2\hat{\beta}^2}{\hat{\delta}}$  and  $c_2 = \frac{\hat{\beta}\hat{\mu}}{\hat{\delta}}$ . The values of  $c_1$  and  $c_2$  in one, two and three dimensions are listed in TABLE S1. In the main text, we drop the tilde notation, but still work in the rescaled model.

$d$	$\hat{\beta}$	$\hat{\delta}$	$\hat{\mu}$	$c_1$	$c_2$
1	1	1/2	4	4	8
2	1/2	3/16	2	8/3	16/3
3	1/3	1/10	4/3	20/9	40/9

TABLE S1: Numerical values of the coefficients  $c_1$  and  $c_2$  in one, two and three dimensions. The coefficients are computed using the microscopically derived values of the coefficients  $\hat{\beta}, \hat{\delta}, \hat{\mu}$ .

### CONNECTION TO THE SWIFT-HOHENBERG EQUATION

The equation of motion corresponding to the Ginzburg-Landau model discussed in the main text reads

$$(\alpha - 4|\psi|^2 + 3|\psi|^4)\psi + c_1 \nabla^2 \psi + \frac{c_1}{2} \nabla^4 \psi + c_2 \left( \psi |\nabla \psi|^2 - \nabla \cdot (|\psi|^2 \nabla \psi) + \frac{1}{4} [\psi^* (\nabla \psi)^2 - \nabla \cdot (\psi^2 \nabla \psi^*)] \right) = 0. \quad (\text{S.6})$$

If we constrain  $\psi$  to be real and rescale it by  $\psi = u \left( \frac{c_1}{6} \right)^{1/4}$ , we obtain the following equation for  $u$

$$-(1 + \nabla^2)^2 u - \mu u + \nu u^3 - u^5 + \gamma(u(\nabla u)^2 + u^2 \nabla^2 u) = 0, \quad (\text{S.7})$$

where  $\mu = \frac{2\alpha}{c_1} - 1$ ,  $\nu = 4\sqrt{\frac{2}{3c_1}}$  and  $\gamma = \frac{5c_2}{2\sqrt{6c_1}}$ . Note, that Eq. (S.7) becomes the static cubic-quintic Swift-Hohenberg equation, in the limit  $\gamma = 0$ .

## LINEARISATION AND SOLITON INTERACTIONS

In this section we will show the technical details how the linearised solutions presented in the paper for both the long-range behaviour of the field and the inter-soliton interaction were found. From our numerical solutions it follows that there is a class of solutions which can be described by a real field, thus in the analysis below we can restrict the field  $\psi$  to be real. The resulting equation of motion reads

$$\frac{dV}{d\psi} + c_1(2\nabla^2 \psi + \nabla^4 \psi) - \frac{5c_2}{2}(\psi(\nabla \psi)^2 + \psi^2 \nabla^2 \psi) = 0, \quad (\text{S.8})$$

where  $V(\psi) = \alpha\psi^2 - 2\psi^4 + \psi^6$  is the potential density. However, as we are interested in the behaviour of the soliton far from its center, we write the field as,

$$\psi(r) = \psi_U + \varepsilon(r), \quad (\text{S.9})$$

where we assume the deviation  $\varepsilon$  from the uniform ground state  $\psi_U$  has only radial dependence, is real and is small. We can then proceed by considering the resulting equation of motion for  $\varepsilon$  by neglecting any terms in Eq. (S.8) that are non-linear in  $\varepsilon$ , as they will be negligible at long-range. This results in the linearised equation of motion

$$c_1 \nabla^4 \varepsilon + 2 \left( c_1 - \frac{5c_2 \psi_U^2}{4} \right) \nabla^2 \varepsilon + \left. \frac{d^2 V}{d\psi^2} \right|_{\psi=\psi_U} \varepsilon = 0. \quad (\text{S.10})$$

Let us define the coefficients

$$a = 1 - \frac{5c_2}{4c_1} \psi_U^2, \quad b = \frac{1}{c_1} \left. \frac{d^2 V}{d\psi^2} \right|_{\psi=\psi_U} = \frac{2}{c_1} (\alpha - 12\psi_U^2 + 15\psi_U^4), \quad (\text{S.11})$$

such that the linearised equation of motion reads

$$\nabla^4 \varepsilon + 2a \nabla^2 \varepsilon + b \varepsilon = 0, \quad (\text{S.12})$$

which can be written, by introducing  $\omega = \nabla^2 \varepsilon$ , as a system of coupled differential equations

$$(\nabla^2 + M) \begin{pmatrix} \omega \\ \varepsilon \end{pmatrix} = 0, \quad M = \begin{pmatrix} 2a & b \\ -1 & 0 \end{pmatrix}. \quad (\text{S.13})$$

By linear transformation to the eigenbasis of the matrix  $M$ , the two equations decouple into

$$\nabla^2 \phi + \mu^2 \phi = 0, \quad (\text{S.14})$$

where  $\mu^2 = a \pm i\sqrt{b-a^2}$  are the two eigenvalues of the matrix  $M$ . We identify Eq. (S.14) as the two-dimensional Bessel equation, where for each eigenvalue of  $M$ , the solution in general is given as a superposition of four Bessel functions. Two of the Bessel functions can be discarded directly by considering the asymptotic behaviour at  $r \rightarrow \infty$  and we obtain

$$\phi_+ = A_+ H_0^{(1)}(\mu r) + B_+ H_0^{(2)}(-\mu r), \quad \phi_- = A_- H_0^{(1)}(-\mu^* r) + B_- H_0^{(2)}(\mu^* r), \quad (\text{S.15})$$

where  $H_0^{(1,2)}$  are zeroth order Hankel functions of the first and second kind,  $A_\pm$  and  $B_\pm$  are some constants, and where we have defined  $\mu = \sqrt{a + i\sqrt{b-a^2}}$ , with  $\text{Re}(\mu) > 0$ ,  $\text{Im}(\mu) > 0$ , which is shown for the relevant parameter regime in FIG. S1. The asymptotic behaviour of  $H_0^{(1,2)}(z)$  at  $|z| \rightarrow \infty$  is

$$H_0^{(1,2)}(z) \rightarrow \sqrt{\frac{2}{\pi z}} e^{\pm i(z-\pi/4)}, \quad (\text{S.16})$$

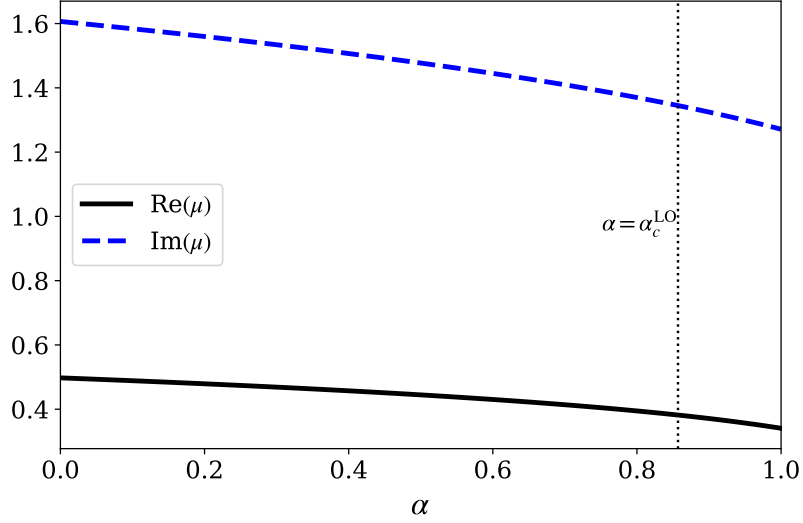


FIG. S1: Plot of the length scale  $\mu$  for the system with changing  $\alpha$  parameter. The inverse of the imaginary part sets the decay length while the inverse of real part sets the oscillation length scale. Note that the transition to the LO state has been marked on the plot by the dotted line.

which means that the inverse of the imaginary part of  $\mu$  sets the decay length scale while the inverse of the real part of  $\mu$  sets the oscillatory length scale. The small deviation  $\varepsilon$  is some superposition of  $\phi_+$  and  $\phi_-$ . However, since  $\varepsilon$  is real valued, we can use that  $\text{Re}(H_0^{(1,2)}(-z^*)) = -\text{Re}(H_0^{(1,2)}(z))$  and thus reduce  $\varepsilon$  to a superposition of  $H_0^{(1)}(\mu r)$  and  $H_0^{(2)}(\mu^* r)$ . Lastly we use that  $H_0^{(2)}(z^*) = (H_0^{(1)}(z))^*$ , which gives us

$$\varepsilon = \text{Re} \left[ C H_0^{(1)}(\mu r) \right], \quad (\text{S.17})$$

where  $C$  is some complex valued constant.

Next we follow the point source approach [38] to determine the intersoliton forces. To that end let us determine the point source  $\rho$  that replicates the asymptotic field  $\varepsilon$  given by Eq. (S.17). The point source is defined by the equation

$$c_1 (\nabla^4 \varepsilon + 2a \nabla^2 \varepsilon + b \varepsilon) = \rho \quad (\text{S.18})$$

and can be found by considering the limit  $|\mathbf{x}| = r \rightarrow 0$ , where  $H_0^{(1)}(\mu|\mathbf{x}|) \rightarrow \frac{2i}{\pi} \ln |\mathbf{x}|$ . Using that  $\nabla^2 \ln |\mathbf{x}| = 2\pi \delta(\mathbf{x})$  we find

$$\nabla^2 H_0^{(1)}(\mu|\mathbf{x}|) = 4i\delta(\mathbf{x}) - \mu^2 H_0^{(1)}(\mu|\mathbf{x}|), \quad (\text{S.19})$$

$$\nabla^4 H_0^{(1)}(\mu|\mathbf{x}|) = 4i\nabla^2 \delta(\mathbf{x}) - 4i\mu^2 \delta(\mathbf{x}) + \mu^4 H_0^{(1)}(\mu|\mathbf{x}|), \quad (\text{S.20})$$

where we have used that  $(\nabla^2 + \mu^2)H_0^{(1)}(\mu|\mathbf{x}|) = 0$  for  $\mathbf{x} \neq \mathbf{0}$ . Inserting these results into Eq. (S.18) gives the point source

$$\rho = -4c_1 \left( \left[ C_I a - C_R \sqrt{b - a^2} \right] \delta(\mathbf{x}) + 4C_I \nabla^2 \delta(\mathbf{x}) \right), \quad (\text{S.21})$$

where  $C = C_R + iC_I$ .

Having calculated the appropriate point source, we now consider two solitons, centred around  $\mathbf{x}_1$  and  $\mathbf{x}_2$  respectively, where the distance  $|\mathbf{x}_1 - \mathbf{x}_2|$  is large. To estimate the interaction between the two solitons, we assume that the total field  $\psi$  is given by the superposition  $\psi(\mathbf{x}) = \psi_U + s_1(\mathbf{x}) + s_2(\mathbf{x})$ , where  $s_j$  is the deviation from the ground state  $\psi_U$  for one soliton, centred around  $\mathbf{x}_j$ . That is  $s_j(\mathbf{x})$  approaches  $\varepsilon_j(\mathbf{x})$  far from its center. The main assumption here is that field of the first soliton at the position of the second is the same as it would have been if there were no soliton there, and vice versa. This is quite a crude approximation since the centers contributes significantly to the interaction energy. The interaction energy  $F_{\text{int}} = F_{12} - F_1 - F_2$  is derived by expanding to first order in the value of  $s_1$  near  $\mathbf{x}_2$  and vice versa. After several integrations by parts we can get rid of the exact solitons  $s_{1,2}$  in favor of their asymptotics  $\varepsilon_{1,2}$ , resulting in the interaction energy

$$F_{\text{int}} = - \int_{\mathbb{R}^2} \rho_1 \varepsilon_2 dxdy = - \int_{\mathbb{R}^2} \rho_2 \varepsilon_1 dxdy. \quad (\text{S.22})$$



By using the derived expression for the asymptotic in Eq. (S.17) and the point source in Eq. (S.21) we find

$$F_{\text{int}} = -4c_1 \sqrt{b - a^2} \text{Re} \left( C^{(1)} C^{(2)} H_0^{(1)}(\mu |\mathbf{x}_1 - \mathbf{x}_2|) \right), \quad (\text{S.23})$$

where  $C^{(1,2)}$  are the constants associated with the two soliton asymptotics respectively. The oscillatory nature of  $H_0^{(1)}$  implies that the solitons will be weakly bound at large distances.